MAC EUROPE 1991 CAMPAIGN: DESIGN AND PERFORMANCE EVALUATION OF AN ACTIVE RADAR CALIBRATOR

S. Ponte
Faculty of Engineering, University of Naples "Federico II"
Napoli, Italy

F. Posa
c/o Physics Dept., Polytechnic of Bari
Bari, Italy

V. Schena, S. Vetrella
Consortium for Research on Advanced Remote Sensing Systems (Co.Ri.S.T.A.)
Napoli, Italy

ABSTRACT

This paper describes the characteristics and performance of an Active Radar Calibrator (ARC) used during the MAC Europe 1991 Campaign conducted in Southern Italy (Matera) to calibrate the Airborne Synthetic Aperture Radar (AIRSAR) and Topographic Synthetic Aperture Radar (TOPSAR) instruments which were flown onboard the NASA/JPL-DC8 aircraft. The main design considerations and the ARC hardware performance are presented. The laboratory measured values of radar cross section and propagation delay time are compared to those obtained from the images acquired during the flight. The TOPSAR raw data have been compressed with a Range-Doppler processor which includes range migration correction. The radiometric calibration, performed with the intensity integration method, gave a backscattering coefficient accuracy of ±0.8 dB. The ARCs' radar cross-sections extracted from the calibrated images have been compared with the laboratory experimental data, giving results in good agreement with the anechoic chamber tests. The laboratory tests gave an absolute calibration error of ±0.6 dB.

Keywords: Active Radar Calibrator, Performance Evaluation, Radiometric Calibration, SAR Processing

1. INTRODUCTION

The Active Radar Calibrator (ARC) is a versatile and useful tool for external calibration of SAR images, due to its design flexibility, reduced dimensions, relatively small sensitivity to positioning errors, large and adjustable Radar Cross Section (RCS) and fully polarimetric capabilities. An ARC is essentially a high gain amplifier coupled with a receiving and a transmitting antenna, which reradiates the received radar signal, with different polarization when requested, towards the (airborne or spaceborne) SAR sensor. The "absolute" backscatter reference given by an ARC has been widely used in past airborne SAR campaigns with the objective of achieving absolute calibration (Refs. 1, 2). The variable polarization signature, easily accomplished by relative rotation of the two antennas, has been effectively used to derive the amplitude and phase characteristics of multichannel polarimetric SARs by means of Polarimetric ARC (PARC) devices (Ref. 3). Furthermore, the high calibration accuracy (typical values are 0.1÷0.5 dB) make the ARC suitable for evaluating in-flight antenna patterns, by using either ARCs (Ref. 4) or PARCs (Ref. 5). The ground calibration plans of future missions such as SIR-C/X-SAR (Ref. 6) require an extensive use of ground-based active calibrators, whereas operating sensors are being very accurately characterized in terms of system performance by using sophisticated and reliable ARCs, such as those used for ERS-1 mission (Ref. 7).

This paper is addressed to the description and the performance analysis of the ARCs developed under a collaboration between the Italian Consortium for Research on Advanced Remote Sensors (Co.Ri.S.T.A.) and the Polytechnic of Bari (Italy), and deployed on the Matera test-site in June 1991, during the MAC Europe Campaign. After a short description of the campaign, the main design considerations of the transponder are presented. Next, a comparison between the laboratory measurements and on-site performance is carried out by analyzing the C-band calibrated data. The concluding remarks point out some considerations about the use of active devices for SAR external calibration campaigns.

2. 1991 CAMPAIGN

In the framework of the MAC Europe 1991 campaign, SAR raw data were gathered by the NASA DC-8 AIRSAR instrument, augmented with a pair of C-band antennas displaced across track, in order to obtain interferometric fringes and topographic information from the imaged surface (TOPSAR, Ref. 8). The test-site was covered five times, with three descending and two ascending runs. Table 1 shows the TOPSAR system parameters of interest for radiometric calibration.

Frequency	5.2875 GHz (C-band)
Wavelength	5.65 cm
Aircraft speed	214.4 m/s
Side-looking angle (ϑ)	45° (nominal); 30°-60°
Altitude	≅9 km
Swath width	4630 m (slant range)
Slant range	11200 m (ϑ=45°)
Ground range resolution	5.30 m
Slant range resolution	3.75 m
Azimuth resolution	0.8 m (1 look, nominal)
Chirp bandwidth	40 MHz
Pulse length	5.0 μs
Sampling frequency	90 MHz
SNR (distributed targets)	13 dB
SNR (point targets)	18 dB
PRF	567 Hz

Table 1: *TOPSAR radar system parameters*

The Matera test-site, in Southern Italy, extends over about 128 km², and consists of prevailingly bare soil, except for two small hilly areas with argillaceous formations. In conjunction with the flight (June 25th, 1991), an extensive ground truth campaign has been carried out, addressed to the classification of 50 sample areas and to the evaluation of texture, soil moisture content and surface roughness on 26 sample points, in correspondence of the location of 26 calibration devices (Ref.9). The point targets are three ARCs and 23 triangular trihedral Corner Reflectors (CR), subdivided in 15, five and three with leg lengths of 95, 150 and 70 cm, respectively. Fig. 1 shows the deployment scheme of the CRs and ARCs on the test-site: the two parallel lines in the horizontal (range) direction were at a distance of 800 m, with a spacing of 200 m between two successive CRs, to avoid coupling effects. All the point targets were deployed on a homogeneous background. The mean temperature during the TOPSAR overpass was 30° C.

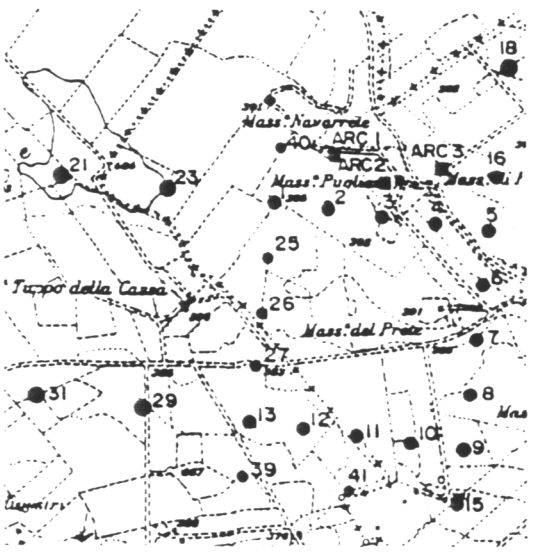

Figure 1: *Istituto Geografico Militare Italiano (IGMI) map of the test site, with the deployment scheme of all Corner Reflectors and ARCs*

3. ARC CONFIGURATION AND HARDWARE PERFORMANCE

Fig. 2 shows a block diagram of the C-band ARC used in the Matera experiment. It basically consists of a receiving antenna and a transmitting antenna coupled with a RF amplifier, together with signal detection circuitry, in order to feed a small part of the received power to a digital section capable of acquiring the in-flight azimuth antenna pattern (Acquisition Section).

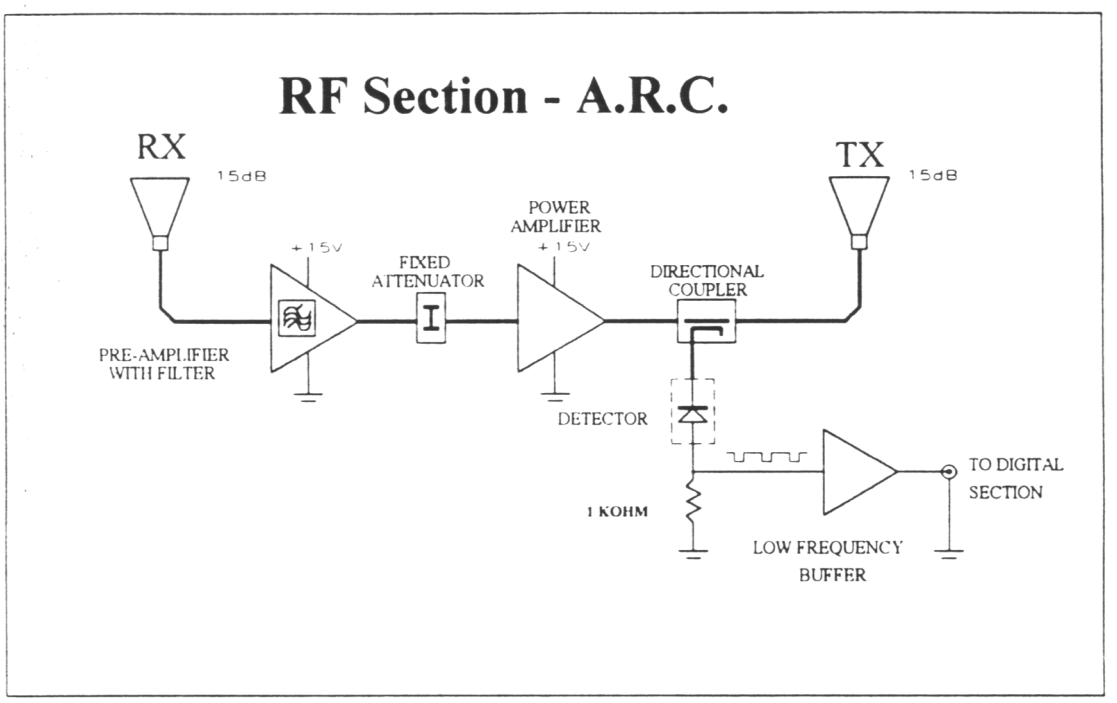

Figure 2: *ARC block diagram*

The receiving antenna is connected to a pre-amplifier, built in hybrid technology and cascaded with a bandpass filter, centred on 5.3 GHz and with a bandwidth of 300 MHz, chosen as a compromise between the need of filtering out spurious signals and noise, and the possibility of using the same ARC for future or different SAR systems. A fixed attenuator arranges the dynamic range of the received signal between the two amplification stages. A variable attenuator has been used, in order to provide a range of RCS values and to avoid saturation of the SAR impulse response function and positive feedback in the RF section. A directional coupler collects a fraction of the received power (10 dB below the input signal level) which is fed to a detector diode. The envelope of the radar signal is demodulated and a negative pulse train at the Pulse Repetition Frequency (PRF) is achieved, with a duty cycle dependent on the SAR system (0.3% for the TOPSAR system). Finally, the signal is transmitted to the synthetic aperture radar via a standard C-band horn, with the same characteristics of the receiving horn. The ARC has been developed with a modular concept, particularly for the signal detection unit, allowing a complete interchangeability between electronical and mechanical components.

ARCs Nos. 1 and 2 have the same hardware characteristics, while ARC No. 3 has been realized without the preamplifier and with the two antennas closer each other. The reduced RCS value (about 15 dBm^2 less than ARCs 1 and 3) could not satisfy the >20-dB requirement on signal-to-clutter ratio necessary to avoid that the ARC's response is hidden in the background return (Ref. 10). However, by properly deploying such an active calibrator, both precision and accuracy in evaluating radiometric bounds for the linear region of the SAR system transfer function could be improved, in order to reduce the error budget (Ref. 11).

In the following we give a short synthesis of the main aspects and characteristics of the ARC:

• **Packaging.** The ARC is a compact device which weighs about 20 kg. Electronics and antennas are weatherproof and the structure is able to withstand normal winds without readjustment. The deployment and orientation are easily accomplished,

and the adjusting/locking mechanisms are manual, independent for each antenna which can be oriented at 45°, 90°, 180° with respect to the other.

• **Power requirements.** Lead-gel airtight rechargeable batteries supply 24V, 10 Ah, and an electronic power regulator supplies 15 V DC to the RF section. The power supply is sufficient to operate at full capacity for 10 hours continuously, with a current absorption of 700 mA. The external power source is easy to connect and to replace, with circuitry to protect against wrong insertions.

• **Amplifier section.** A LED turns on when the ARC is receiving a power greater than or equal to the peak expected power. Both the preamplifier and the power amplifier have gain flatness of ±0.05 dB over the 300 MHz bandwidth, with a noise figure of 3.6 dB at the central frequency of 5.3 GHz. Table 2 and Fig. 3 show the laboratory tests on both the preamplifier (Model JCA56-353) and the power amplifier (Model JCA56-519), and the gain curves over the available bandwidth. In agreement with the manufacturer's data, the return and mismatch losses at 5.3 GHz have been found to be 16.5 dB and less than 0.1 dB, respectively. The one-dB compression point of the cascaded amplifiers is when the input power is -40 dBm, and the linearity range is 30 dBm, from -70 to -40 dBm input power.

MODEL N.	JCA56-353 (Pre-Amp)
DC SUPPLY	+15 Vdc

Frequency [GHz]	**Gain [dB]**	**Noise figure [dB]**	**Input VSWR**	**Output VSWR**	**Compression @+10 dBm**
5.15	see	3.5	1.84	1.24	2
5.25	plot	3.6	1.41	1.23	2
5.45	(Fig. 4a)	3.5	1.27	1.24	2

MODEL N.	JCA56-519 (Power Amp)
DC SUPPLY	+15 Vdc

Frequency [GHz]	**Gain [dB]**	**Noise figure [dB]**	**Input VSWR**	**Output VSWR**	**Compression @+25 dBm**
5.00	see	3.4	1.16	1.50	8
5.30	plot	3.6	1.35	1.50	7
5.60	(Fig. 4b)	3.8	1.60	1.60	7

Table 2: *Results of the laboratory tests on the RF section (pre-amplifier and power amplifier)*

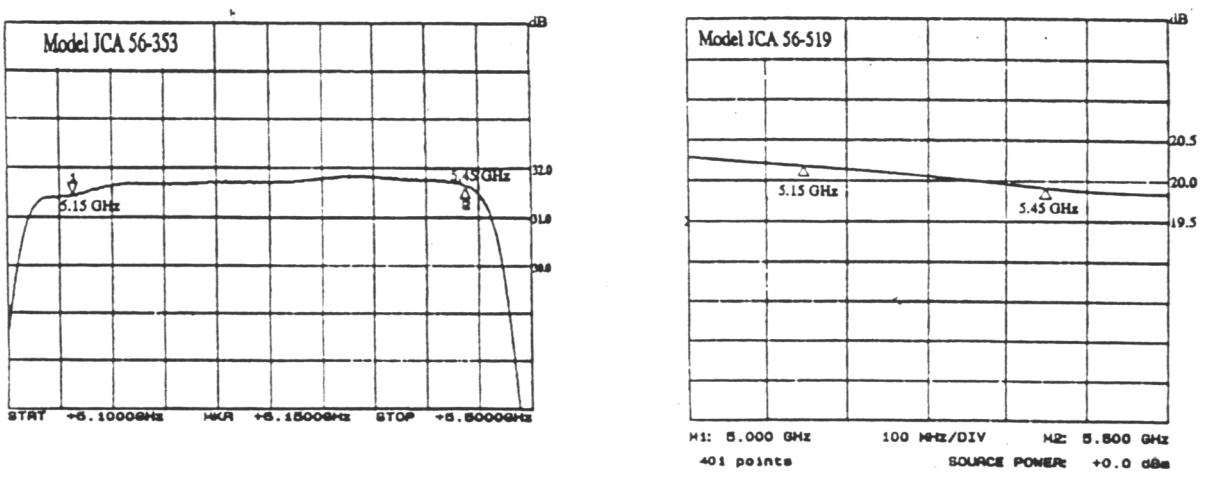

(a) (b)

Figure 3: *Measured frequency response of the preamplifier (a) and of the power amplifier (b)*

The temperature test chamber measurements detected a relative variation of the gain over temperature of 5.7%, i. e., 0.08 dB/°C. Fig. 4 shows the RCS of the ARC as a function of temperature, from -10° C to +40° C, at 5° C increments, with an input power of -60 dBm, which is located in the central region of the allowable input dynamic range. This characteristic affects the RCS during the operation of the ARC which requires the thermal compensation of both the RCS and the received power values through a look-up table.

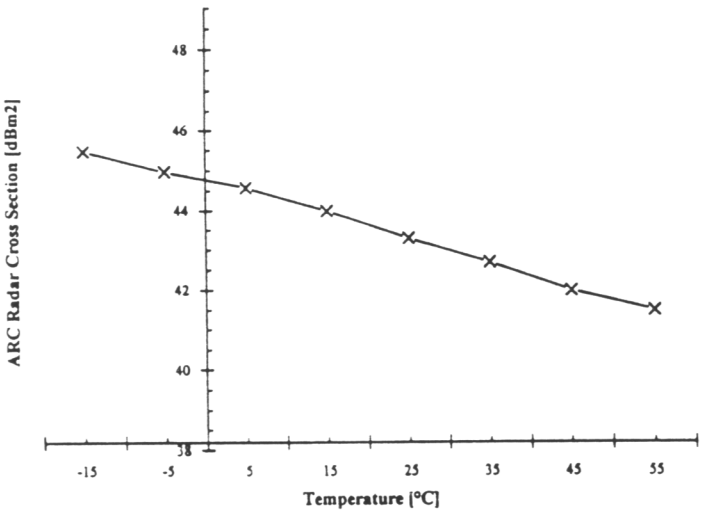

Figure 4: *Climatic room tests: diagram of radar cross-section over temperature. The input power level is -60 dBm*

• **Antennas.** Both RX and TX antennas, labeled for easy identification, are C-band pyramidal horns with rectangular aperture (13.2x9.4 cm). The -3 dB beamwidths in the E and H-planes are respectively 25° and 34°, values which overcome orientation problems. To achieve a good cross-coupling performance, the distance between the center of simmetry of the two horns has been set to 62 cm. At the central frequency of 5.3 GHz, the antennas have a bandwidth of 300 MHz. The peak gain declared by the manufacturer is 15 dB, with typical sidelobes level of -20 dB which allows to minimize multipath effects and background noise. In addition to the orientation of the antennas with respect to the flight line, a different polarization state is achieved by rotating each antenna about its boresight at 45° steps, with a system of hexagonal-head bolts on a frame structure. The minimal cross-polarization isolation is 32 dB. Echo-absorbing material surrounds the horns, in order to avoid resonance effects and to minimize the re-radiation effects of the structure (see Fig. 5). The decoupling between the antennas, defined as $10\log_{10}(P_p^t / P_q^r)$, where P_p^t is the transmitted power with polarization state p, and P_q^r is the power received with polarization q, is >80 dB in the HV and VH configurations, >60 dB in the VV orientation, and >54 dB in the HH mode. The mismatch loss is less than 0.05 dB and the return loss is 20 dB, with a corresponding voltage standing wave ratio (VSWR) of 1.22.

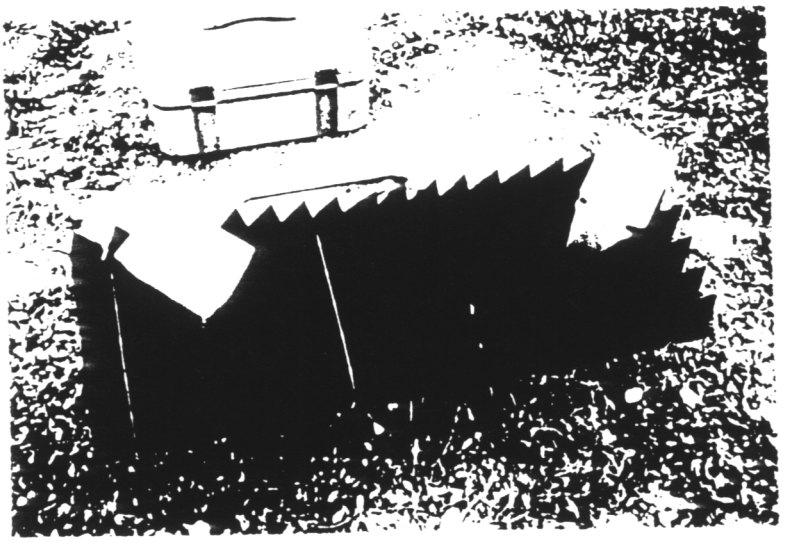

Figure 5: *ARC structure*

4. ARC PERFORMANCE EVALUATION

In order to validate the laboratory measurements of the main ARC parameters, we performed a full compression and radiometric calibration of the SAR raw data acquired by the two antennas of the TOPSAR instrument. The raw data were focused in the frequency domain, with a Range-Doppler processor, developed by Co.Ri.S.T.A.. The range reference function emulated the on-board Digital Chirp Generator (DCG), and the compressed data were frequency-shifted at baseband, to remove the video offset frequency. The Hamming-weighted azimuth reference function was of variable length, depending on the incidence angle. The range migration was not negligible (about 2 range bins at a mean incidence angle of 47.5°), and it was corrected by a frequency-domain trajectory restoration algorithm, based on clutterlock/autofocus algorithms and on resampling techniques by means of *sinc* weighting functions. Multiple pixel averaging of the intensity images (1024x1024 pixels) was performed to achieve a square pixel (Fig.6). Slant range and azimuth spacings are 3.33 m and 3.03 m respectively.

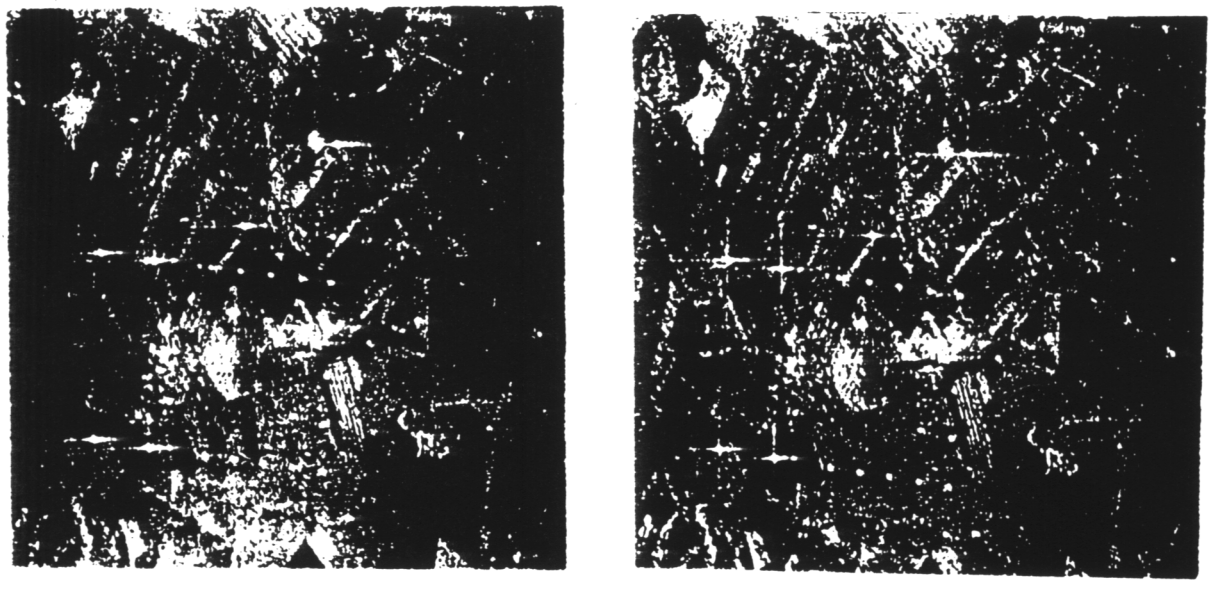

(a) (b)

Figure 6: *Image of the test site obtained from raw data gathered by antenna 1 (transmitting/receiving) (a) and antenna 2 (receiving) (b)*

Unfortunately, ARC No. 2 did not work during the TOPSAR overpass, due to a hardware malfunctioning, and it is not visible, while ARCs Nos. 1 and 3 are clearly recognizable above the upper horizontal line of corner reflectors. Fig. 7 shows a three-dimensional plot of the ARC response, with z-axis representing amplitudes in dB.

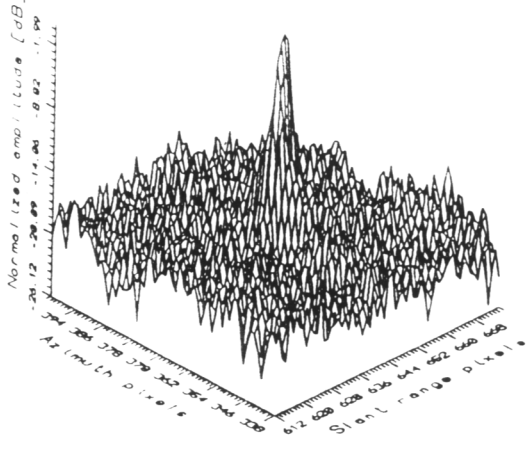

Figure 7: *Three-dimensional representation of the response of ARC No. 1*

A set of standard quality tests were conducted to test the processor performance, in terms of one-dimensional resolution, Integrated Sidelobe Ratio (ISLR) and Peak Sidelobe Ratio (PSLR) in both range and azimuth directions (Tab. 3).

ARC No.	ϑ_i [deg]	ρ_{gr} [m]	ρ_{sr} [m]	Range ISLR [dB]	Range PSLR [dB]	ρ_{az} [m]	Azimuth ISLR [dB]	Azimuth PSLR [dB]
1	46.3	5.61	4.06	-8.95	-11.16	8.82	-18.69	-27.22
3	47.6	5.67	4.19	-6.44	-9.68	8.68	-12.61	-17.75
1	46.3	5.87	4.24	-9.38	-25.42	8.82	-16.75	-16.07
3	47.6	5.29	3.90	-7.59	-11.79	7.71	-11.07	-13.52

Table 3: *Ground range (ρ_{gr}), slant range (ρ_{sr}) and azimuth (ρ_{az}) resolutions, ISLR and PSLR in range and azimuth directions for ARCs Nos. 1 and 3. The mean broadening factors are 15% in range and 25% in azimuth. Second column reports the calculated incidence angle (ϑ_i)*

The radiometric calibration of the images was performed by using the intensity integration method (Ref. 12), which is insensitive to misfocussing and to scene and/or processor coherence. After having estimated $\mathcal{E}_{gp}$, the integrated energy associated to the reference target (a CR), $\mathcal{E}_{gu}$, the background clutter energy, and the image noise power, the average backscattering coefficient $<\sigma^0>$ in correspondence of each point target was evaluated by applying the equation:

$$<\sigma^0> = \sigma_{ref} \frac{\mathcal{E}_{gu}}{A_u \mathcal{E}_{gp}} \sin\vartheta_u \qquad (1)$$

where $A_u = \delta_{sr}\delta_{az}$ is the uniform target area, given by the product of the slant range and azimuth spacings δ_{sr} and δ_{az}, ϑ_u is the incidence angle of the uniform target area, σ_{ref} is the reference RCS value of the CR. The error on each σ^0 determination is associated to the integral estimate of the point target energy ($\mathcal{E}_{gp}$), and it depends on the speckle autocovariance function (Ref. 13), integrated over the area A_p, containing the point target response function. We found for the standard deviation of $\mathcal{E}_{gp}$, and therefore for the calibration accuracy of the method, a mean value of 0.7 dB. The reference RCS value and the estimate of the energy term $\mathcal{E}_{gp}$ were derived from the eleven C-band CRs (95-cm leg length) deployed on the test-site: we chose the CR deployed on the area with the smallest standard deviation of the background clutter (0.02 dB, CR no. 5). On the amplitude image (proportional to $\sqrt{\sigma^0}$) obtained from the pixel-by-pixel calibration algorithm, we derived the values of σ for ARC No. 1 by evaluating the product $\mathcal{E}_{gp}A_p$ on the area containing the ARC response. The theoretical RCS (30.3 dBm^2) of the eleven CRs was derived within ± 0.8 dB, which consequently represents the minimal accuracy in the estimation of σ.

A further step was the estimation of the ARC delay time, which was obtained by measuring the ground range R_G of CR No. 40, that is the nearest to ARC No. 1 (Fig. 8 depicts the geometry), and comparing this value with the Universal Transverse Mercator (UTM) co-ordinates known after the ground truth information, in order to compensate local bias effects due to geometric errors such as scale and skew. We evaluated R_G of the ARC and, after removal of geometric distortion effects estimated on the CR, we got the ground range difference between the location on the image and the actual position of the ARC. This offset was converted to a slant range displacement of two range bins, which corresponds (see Table 1) to a delay time of 44 ns.

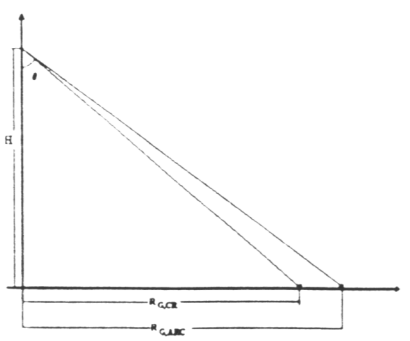

Figure 8: *Geometry for the evaluation of the ARC's delay*

5. RESULTS

An extensive set of anechoic chamber measurements have been carried out on the ARCs, and RCS and delay time of the active devices were evaluated on the compressed data with the techniques described in the previous section. A synoptic view of nominal, laboratory and calibration results is shown on Table 4 for ARC No. 1.

	Nominal Value	Laboratory Measurement	Measurement on calibrated SAR Images
Antenna Gain [dB]	15	16.0±0.6	-
RF Gain [dB]	51.2	49.2±0.6	-
RX-TX decoupling [dB]	>60 (VV) >54 (HH) >80(VH,HV)	~70 (VV)	-
RCS [dBm²]	45.2	43.28±0.6	43.6±0.8
Delay time [ns]	-	30±0.5	44±11

Table 4: *Results: nominal values, laboratory measurements and estimated values from SAR images*

The first row reports the antenna gains. At boresight, the combined gain $G_{r,ARC} \cdot G_{t,ARC}$ of the ARCs' receiving and transmitting antennas, has been found to be 32.0 dB, measured with a standard-gain test antenna. The second row shows the laboratory measurements of G_a, the RF gain, performed at room temperature (22.5 °C). The differences from the nominal values are ascribable to the sum of L_{ATT}, the attenuator insertion loss, and L_{MIS}, the overall mismatch loss, which was 1.0 + 0.97 dB. The cross-polarization isolation measurements (HH and HV modes) gave a value below 32 dB, troughout the dynamic range. The third row reports the decoupling measurements, in different polarization configurations. The measured gain values have been used to evaluate σ_{ARC}, the peak RCS, with the basic equation (Ref. 14):

$$\sigma_{ARC} = \frac{\lambda^2}{4\pi} \frac{G_{r,ARC} G_{t,ARC} G_a}{L_{ATT} L_{MIS}} \qquad (2)$$

where λ is the wavelength. The laboratory results, on the fourth row of Table 4, gave an RCS which satisfies the ±1dB precision requirement on a bare soil background (Ref. 15). The absolute radiometric bias factor K, defined after (1) as:

$$K = \frac{\sigma_{ref}}{A_u \mathcal{T}_{sp}} \qquad (3)$$

was 52.4 dB. The RCS values have also been calculated by using the two radiometrically corrected images, and Table 4 reports the mean value.

The error budget on the laboratory calibration of the ARCs gave on the estimated accuracy on the RCS a value of ±0.6 dB. Error sources are summarized as follows:

- measurement accuracy due to the gain-measuring system: 0.2÷0.3 dB;
- antenna gain instability over temperature, evaluated by using the manufacturer's data: 0.1 dB;
- thermal noise, antenna pointing errors, multipath errors: ±0.2÷0.3 dB.

Finally, in far-field conditions, by positioning the active devices about 20 m away from the measurement equipment, we measured the propagation delay of each ARC, obtaining a value of 30±5 ns. The corresponding delay time (ARC No. 1)

measured on the images is shown in the last row of Table 4. The accuracy of the delay measurement on the SAR images is δ_τ/c, where c is the velocity of light, and is ±11 ns.

6. CONCLUDING REMARKS

We have presented the design considerations and the validation strategy of an ARC, a high-and-tunable-RCS point target which can guarantee an accurate radiometric and geometric calibration of a SAR system, overcoming the stability and size problems of passive calibrators with the same RCS values. ARCs have some drawbacks, such as the relatively high cost, the inability of measuring the SAR transfer funtcion far from the high end of the allowable dynamic range, and therefore the risk of saturation on the digitized image, due to their high RCS. Nevertheless, ARCs have special characteristics which make them unique as external calibration devices, such as:

- the possibility of collecting a small portion of the received signal and feeding it to a Ground Receiver, or Acquisition, Section, capable of monitoring the in-flight azimuth antenna pattern by detecting the field strength during the synthetic aperture formation time;

- high signal-to-clutter ratios (SCR) in critical situations where a dark background (i.e. low σ^0) is not available;

- the availability of measurements of the SAR cross- and co-polarized transfer characteristics without different deployments;

- the variability of the propagation delay due to the waveguides and electronics of the RF section. This delay could be controlled in order to force the point target response in a more convenient location in the final image. For example, the ARC could be placed on the edge of a quasi-absorbing surface (a small lake or a large uniform field), and by inserting a suitable value of the delay time, the active device would be imaged on areas with very low backscattering;

- the possibility of inserting controlled phase errors on the interferometric data, by tuning the delay time. This could be a useful feature for interferometric phase calibration and for the estimation of processor-induced phase errors.

Currently, successful laboratory tests on a prototype ground acquisition section, interfaced to a PC, allow us to use the ARC with azimuth pattern recording features, and an X-band ARC with its Acquisition Section is being developed and tested. Future developments on our ARCs concern a better characterization of the error sources and a reduction of the absolute calibration error, together with the thermal stabilization of the RF section, mandatory when using the active calibrator as a ground receiver.

ACKNOWLEDGEMENTS

This work has been partly supported by the Italian Space Agency (ASI) under the contract ASI-90-RS70. Special thanks are due to Dr. E. Serena and Mr. G. Spaccarelli of Alenia Spazio for their contribution to the ARC's testing.

REFERENCES

1. Hartl P, Reich M, Bhagavathula S. 1987, An Attempt to Calibrate Air-borne SAR Images Using Active Radar Calibrators and Ground Based Scatterometers, *Proc. IGARSS '87 Symposium*, Ann Arbor, MI, pp. 501-508

2. Holt J, Freeman A 1990, Calibration of Bonanza Creek, Alaska, SAR Imagery Using Along-Track Calibration Targets, *Proc. IGARSS '90*, College Park, Maryland, Vol. III, pp. 2309-2312

3. Freeman A, Shen Y & Werner C L 1990, Polarimetric SAR Calibration Experiment Using Active Radar Calibrators, *IEEE Trans. Geosc. & Remote Sensing*, Vol.28, No. 2, pp. 224-240

4. Dobson M C, Ulaby F. T., Brunfeldt D. R. & Held D. N. 1986, External Calibration of SIR-B Imagery with Area-Extended and Point Targets, *IEEE Trans. Geosc. & Remote Sensing*, Vol. GE-24, No. 4, pp. 453-461

5. Seifert P., Lentz H., Zink M. & Heel F. 1992, Ground-Based Measurements of Inflight Antenna Patterns for Imaging Radar Systems, *IEEE Trans. Geosc. & Remote Sensing*, Vol. 30, No. 6, pp. 1131-1136

6. Freeman A. 1990, *SIR-C Ground Calibration Plan*, JPL D-6999

7. Woode A. D., Desnos Y.-L. & Jackson H. 1992, The Development and First Results from the ESTEC ERS-1 Active Radar Calibration Unit, *IEEE Trans. Geos. & Remote Sensing*, Vol. 30, No. 6, pp. 1122-1130

8. Zebker H. A., Madsen S. N., Martin J., Wheeler K. B., Miller T., Lou Y, Alberti G., Vetrella S., Cucci A. 1992, The TOPSAR Interferometric Radar Topographic Mapping Instrument, *IEEE Trans. Geosc. & Remote Sensing*, Vol 30, No. 3, pp. 933-940

9. Co.Ri.S.T.A.-AQUATER 1992, *Progetto SAR 1991: Rapporto Finale Campagna AGRISAR '91*, Co.Ri.S.T.A. internal document

10. Blacksmith P. Jr., Hiatt R. E., Mack R. B. 1965, Introduction to Radar Cross Section Measurement, *Proceedings of the IEEE*, Vol. 53, pp- 901-920

11. De Carolis G., Posa F., Veneziani N. 1991, Estimation of Linearity and Confidence Level for the SAR Radiometric Transfer Function, *Proc. 11th EARSeL Symposium*, Graz (Austria), pp. 130-139.

12. Gray A. L., Vachon P. W., Livingstone C. E. & Lukowski T. I. 1990, Synthetic Aperture Radar Calibration Using Reference Reflectors, *IEEE Trans. Geosc. & Remote Sensing*, Vol. GE-28, pp. 374-383

13. Ulander L. M. H. 1991, Accuracy of Using Point Targets for SAR Calibration, *IEEE Trans. Aerosp. & Elec. Syst.*, Vol. 27, No. 1, pp. 139-148

14. Brunfeldt D. R. & Ulaby F. T. 1984, Active Reflector for Radar Calibration, *IEEE Trans. Geos. & Remote Sensing*, Vol GE-22, No. 2, pp. 165-169

15. Ulaby F. T., Moore R. K. & Fung A. K. 1982, *Microwave Remote Sensing: Active and Passive*, Vol II, Addison-Wesley, Reading, MA